Supplementary Material for "Strain-enabled control of chiral magnetic structures in MnSeTe monolayer"

Zhiwen Wang(王智文)[1,2], Jinghua Liang(梁敬华)[2], Hongxin Yang(杨洪新)[1,2*]

[1] National Laboratory of Solid State Microstructures, School of Physics, Collaborative Innovation Center of Advanced Microstructures, Nanjing University, Nanjing 210093, China

[2] Ningbo Institute of Materials Technology and Engineering, Chinese Academy of Sciences, Ningbo 315201, China

Part I. The variation of magnetic moment under biaxial strain

To show a complete understanding of the variation of magnetic moment under biaxial strain. We have calculated the spin magnetic moment of each element in MnSeTe as a function of biaxial strain, as seen in Fig. S1.

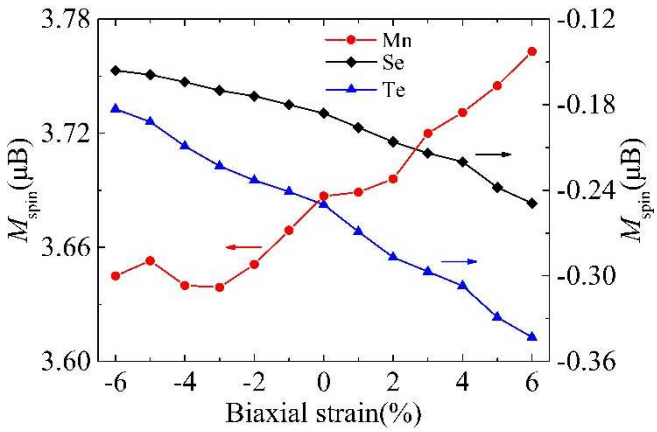

Figure S1. The spin magnetic moment of Mn, Se and Te elements as a function of biaxial strain in MnSeTe monolayer.

As we can see from Fig. S1, the main contribution to magnetism of MnSeTe comes from the Mn atoms, meanwhile, Se and Te are both effectively spin-polarized due to the hybridizations between Mn-*d* and Se(Te)-*p* orbitals. The magnetic moments of Se and Te elements decreases rapidly when tensile strain is applied, while increases monotonously with a compressive strain. With the increment of tensile strain, however, the magnetic moment of Mn atom enhances. Interestingly, the magnetic moment reduces for compressive strain smaller than -3%, while increases as the strain larger than -3%.

*hongxin.yang@nju.edu.cn

Part II. The relationship between orbital magnetic moment and MAE

To investigate the impact of orbital contributions to the MAE, we have calculated the difference of the local orbital moments with the direction of magnetization along in-plane ($M_{\perp}$) or out-of-plane($M_{//}$) axis of MnSeTe plane. We define the difference $\Delta M_{orbital} = M_{\perp} - M_{//}$, which the Fig. S2 shows the results.

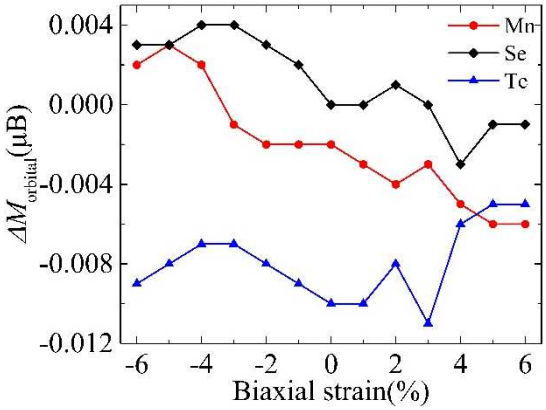

Figure S2. The difference of the local orbital moments $\Delta M_{orbital}$ as a function of biaxial strain in MnSeTe monolayer.

From the Fig. S2, we can see that the $\Delta M_{orbital}$ of the Mn, Se and Te elements are smaller than 0.01μ_B per atom. Moreover, the variation of $\Delta M_{orbital}$ for all the elements disagree with the change of MAE under biaxial strain. Therefore, there is no direct relation between orbital magnetic moments and MAE in MnSeTe monolayer.

Part III. The calculation of the nearest-, next-nearest-, and third-nearest-neighbor Heisenberg exchange coupling J_i (i = 1, 2 and 3)

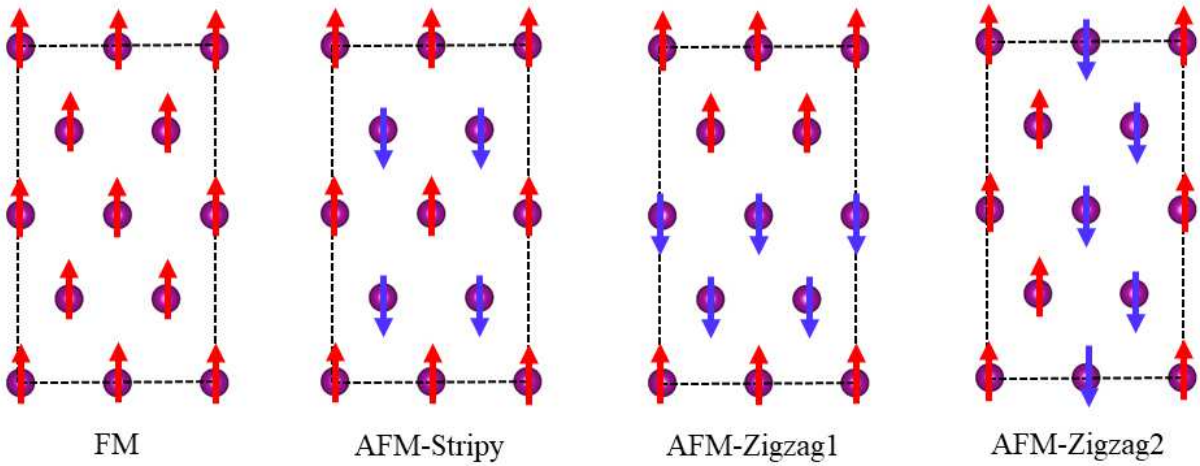

Figure S3. Four different spin configurations used to obtain the exchange coupling parameters. The red and blue arrows mean up-spin and down-spin, respectively. For clarity only the Mn atoms are shown here

To obtain the Heisenberg exchange parameters, we build a $2\times2\sqrt{3}\times1$ supercell and

calculate the energies of four collinear spin configurations shown in Fig. S3. The total energies for these spin configurations are:

$$E_{FM}=E_0-24J_1|\boldsymbol{S}|^2-24J_2|\boldsymbol{S}|^2-24J_3|\boldsymbol{S}|^2 \quad (S1)$$

$$E_{AFM}^{stripy}=E_0+8J_1|\boldsymbol{S}|^2+8J_2|\boldsymbol{S}|^2-24J_3|\boldsymbol{S}|^2 \quad (S2)$$

$$E_{AFM}^{zigzag1/zigzag2}=E_0\mp8J_1|\boldsymbol{S}|^2\pm8J_2|\boldsymbol{S}|^2+8J_3|\boldsymbol{S}|^2 \quad (S3)$$

Therefore, we can obtain the J_i (i = 1, 2 and 3):

$$J_1=\frac{E_{FM}-E_{AFM}^{stripy}+2(E_{AFM}^{zigzag1}-E_{AFM}^{zigzag2})}{-64S^2} \quad (S4)$$

$$J_2=\frac{E_{FM}-E_{AFM}^{stripy}-2(E_{AFM}^{zigzag1}-E_{AFM}^{zigzag2})}{-64S^2} \quad (S5)$$

$$J_3=\frac{2(E_{AFM}^{zigzag1}+E_{AFM}^{zigzag2})-(E_{FM}+3E_{AFM}^{stripy})}{128S^2} \quad (S6)$$

Part IV. Calculation of the nearest-, next-nearest-, and third-nearest-neighbor atomic DMI d_i (i = 1, 2 and 3)

To obtain d_i (i = 1, 2 and 3) we employ with three different supercells including 4×1×1, 5×1×1 and 6×1×1 in our DMI calculations, as shown in Fig. S4, which the Monckhorst-Pack scheme were used for the Γ-centered 5×20×1, 5×25×1 and 4×24×1 k-point sampling, respectively.

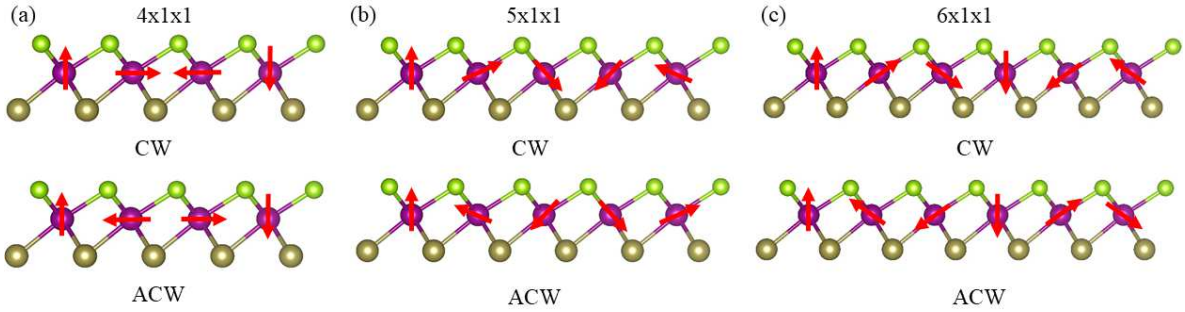

Figure S4. Spin configurations used to calculate the DMI d_i (i = 1, 2 and 3) for the MnSeTe monolayers. The upper panel is clockwise (CW) and the lower panel is anticlockwise (ACW). (a) 4×1×1 supercell (b)5×1×1 supercell (c) 6×1×1 supercell

A. Contributions of the 4×1×1 supercell

As shown in Fig. S5, each atom has the same nearest neighbor atoms in a plane, which result in equal contribution to DMI energy. Thus, we take atom 2 as an example, its total energy can be written as:

$$E_2 = E_2(d_1) + E_2(d_2) + E_2(d_3) + E_{other} \quad (S7)$$

with

$$E_2(d_1)=\frac{1}{2}\left[d_1^{23}(S_2\times S_3)+d_1^{21}(S_2\times S_1)+d_1^{23''}d(S_2\times S_{3''})+d_1^{22''}(S_2\times S_{2''})+d_1^{21'''}(S_2\times S_{1'''})+d_1^{22'''}(S_2\times S_{2'''})\right] \quad \text{(S8)}$$

$$E_2(d_2)=\frac{1}{2}\left[d_2^{23'''}(S_2\times S_{3'''})+d_2^{24''}(S_2\times S_{4''})+d_2^{23'}(S_2\times S_{3'})+d_2^{21''}(S_2\times S_{1''})+d_2^{24'''}(S_2\times S_{4'''})+d_2^{21''''}(S_2\times S_{1''''})\right] \quad \text{(S9)}$$

$$E_2(d_3)=\frac{1}{2}\left[d_3^{22''''}(S_2\times S_{2''''})+d_3^{24}(S_2\times S_4)+d_3^{24}(S_2\times S_4)+d_3^{24''''}(S_2\times S_{4''''})+d_3^{24'}(S_2\times S_{4'})+d_3^{22'}(S_2\times S_{2'})\right] \quad \text{(S10)}$$

where the factor 1/2 is included to account for the DMI energy sharing between the two sites of each bond, and the equations of (S8), (S9), and (S10) represent the contributions of nearest-, next-nearest-, and third-nearest-neighbor DMI in 4×1×1 supercell, respectively. The E_{other} gathers spin independent, anisotropy and symmetric exchange energy contributions.

Considering the spin orientation between S_2 with the other spins, the energies of atom 2 for CW (E_{cw}) and ACW (E_{acw}) spin configurations in Eqs. (S7) can be rewritten as

$$E_{2,\,cw} = \frac{3d_1}{2}\sin\alpha + \frac{\sqrt{3}d_2}{2}\sin\alpha + E_{other} \quad \text{(S11)}$$

$$E_{2,\,acw} = -\frac{3d_1}{2}\sin\alpha - \frac{\sqrt{3}d_2}{2}\sin\alpha + E_{other} \quad \text{(S12)}$$

where the α is $\frac{\pi}{2}$. Using Eqs. (S11), (S12), the total DMI energy in the cell and the value per bond are found to be related by

$$\Delta E_{DMI,\,1} = (E_{cw} - E_{acw}) = 12d_1\sin\alpha + 4\sqrt{3}d_2\sin\alpha \quad \text{(S13)}$$

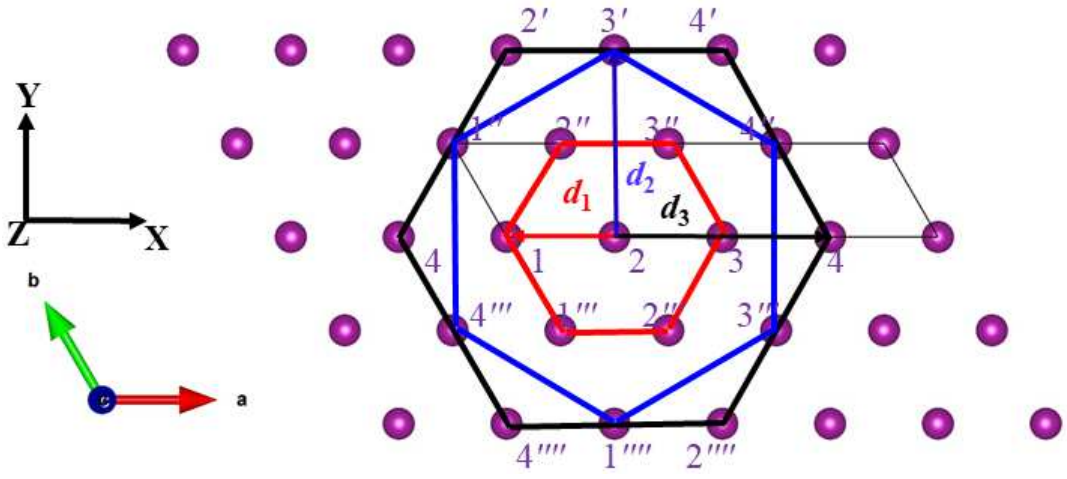

Figure S5. Top view of 4×1×1 supercell used to visualize intralayer contributions into DMI for the Mn layer. For clarity only the Mn atoms are shown here

B. Contributions of 5×1×1 supercell

According to same analysis in 4×1×1 supercell as shown above, we also take atom 2 as an example for 5×1×1 supercell as shown in Fig. S6. The energy of atom 2 can be written as

$$E_2 = E_2(d_1) + E_2(d_2) + E_2(d_3) + E_{\text{other}} \quad \text{(S14)}$$

with

$$E_2(d_1)=\frac{1}{2}[d_1^{23}(S_2\times S_3)+d_1^{21}(S_2\times S_1)+d_1^{23''}(S_2\times S_{3''})+d_1^{22''}(S_2\times S_{2''})+d_1^{21''}(S_2\times S_{1''})+d_1^{22'''}(S_2\times S_{2'''})] \quad \text{(S15)}$$

$$E_2(d_2)=\frac{1}{2}[d_2^{23'''}(S_2\times S_{3'''})+d_2^{24''}(S_2\times S_{4''})+d_2^{23'}(S_2\times S_{3'})+d_2^{21''}(S_2\times S_{1''})+d_2^{25'''}(S_2\times S_{5'''})+d_2^{22''''}(S_2\times S_{2''''})] \quad \text{(S16)}$$

$$E_2(d_3)=\frac{1}{2}[d_3^{23''''}(S_2\times S_{3''''})+d_3^{24}(S_2\times S_4)+d_3^{24'}(S_2\times S_{4'})+d_3^{21''''}(S_2\times S_{1''''})+d_3^{25}(S_2\times S_5)+d_3^{22'}(S_2\times S_{2'})] \quad \text{(S17)}$$

where the equations of (S15), (S16), and (S17) represent the contributions of nearest-, next-nearest-, and third-nearest-neighbor DMI in 5×1×1 supercell, respectively.

The energies of atom 2 for CW (E_{cw}) and ACW (E_{acw}) spin configurations in Eqs. (S14) can be rewritten as

$$E_{2,\text{cw}} = \frac{3d_1}{2}\sin\beta+\frac{\sqrt{3}d_2}{4}(2\sin\beta+\sin 2\beta-\sin 3\beta)+\frac{3d_3}{4}(\sin\beta-\sin 2\beta)+E_{\text{other}} \quad \text{(S18)}$$

$$E_{2,\text{acw}} = -\frac{3d_1}{2}\sin\beta-\frac{\sqrt{3}d_2}{4}(2\sin\beta+\sin 2\beta-\sin 3\beta)-\frac{3d_3}{4}(\sin\beta-\sin 2\beta)+E_{\text{other}} \quad \text{(S19)}$$

where the β is $\frac{2\pi}{5}$. Using Eqs. (S18), (S19), the total DMI energy in the cell and the value per bond are found to be related by

$$\Delta E_{\text{DMI},2}=(E_{\text{cw}}-E_{\text{acw}})=15d_1\sin\gamma+\frac{5\sqrt{3}d_2}{2}(2\sin\gamma+\sin 2\gamma-\sin 3\gamma)+\frac{15d_3}{2}(\sin\gamma-\sin 2\gamma) \quad \text{(S20)}$$

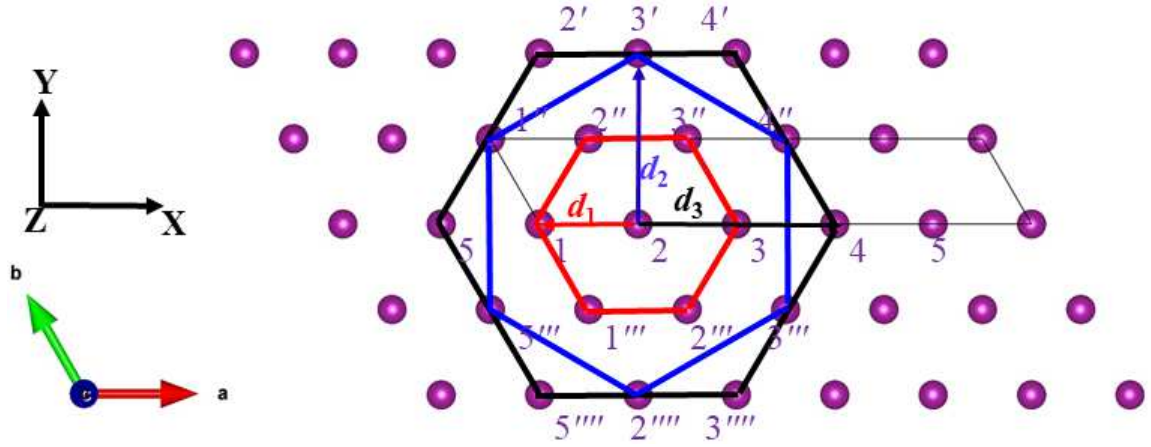

Figure S6. Top view of 5×1×1 supercell used to visualize intralayer contributions into DMI for the Mn layer. For clarity only the Mn atoms are shown here

C. Contributions of 6×1×1 supercell

Again, in 6×1×1 supercell structure, we take atom 2 as an example as shown in Fig. S7, which energy of atom 2 can be written as

$$E_2 = E_2(d_1) + E_2(d_2) + E_2(d_3) + E_{other} \quad \text{(S21)}$$

with

$$E_2(d_1)=\frac{1}{2}[d_1^{23}(S_2\times S_3)+d_1^{21}(S_2\times S_1)+d_1^{23''}(S_2\times S_{3''})+d_1^{22''}(S_2\times S_{2''})+d_1^{21'''}(S_2\times S_{1'''})+d_1^{22'''}(S_2\times S_{2'''})] \quad \text{(S22)}$$

$$E_2(d_2)=\frac{1}{2}[d_2^{23'''}(S_2\times S_{3'''})+d_2^{24''}(S_2\times S_{4''})+d_2^{23'}(S_2\times S_{3'})+d_2^{21''}(S_2\times S_{1''})+d_2^{26'''}(S_2\times S_{6'''})+d_2^{21''''}(S_2\times S_{1''''})] \quad \text{(S23)}$$

$$E_2(d_3) = \frac{1}{2}[d_3^{23''''}(S_2\times S_{3''''})+d_3^{24}(S_2\times S_4)+d_3^{24'}(S_2\times S_{4'})+d_3^{21''''}(S_2\times S_{1''''})+d_3^{25}(S_2\times S_5)+d_3^{22'}(S_2\times S_{2'})] \quad \text{(S24)}$$

Where the equations of (S22), (S23), and (S24) represent the contributions of nearest-, next-nearest-, and third-nearest-neighbor DMI in 6×1×1 supercell, respectively.

The energies of atom 2 for CW (E_{cw}) and ACW (E_{acw}) spin configurations in Eqs. (S21) can be rewritten as

$$E_{2,\,cw} = \frac{3d_1}{2}\sin\gamma+\sqrt{3}d_2\sin\gamma+\frac{3d_3}{2}\sin\gamma+E_{other} \quad \text{(S25)}$$

$$E_{2,\,acw} = -\frac{3d_1}{2}\sin\gamma-\sqrt{3}d_2\sin\gamma-\frac{3d_3}{2}\sin\gamma+E_{other} \quad \text{(S26)}$$

where the γ is $\frac{\pi}{3}$. Using Eqs. (S25), (S26), the total DMI energy in the cell and the value per bond are found to be related by:

$$\Delta E_{DMI,\,3} = (E_{cw} - E_{acw}) = 18d_1\sin\gamma+12\sqrt{3}d_2\sin\gamma+18d_3\sin\gamma \quad \text{(S27)}$$

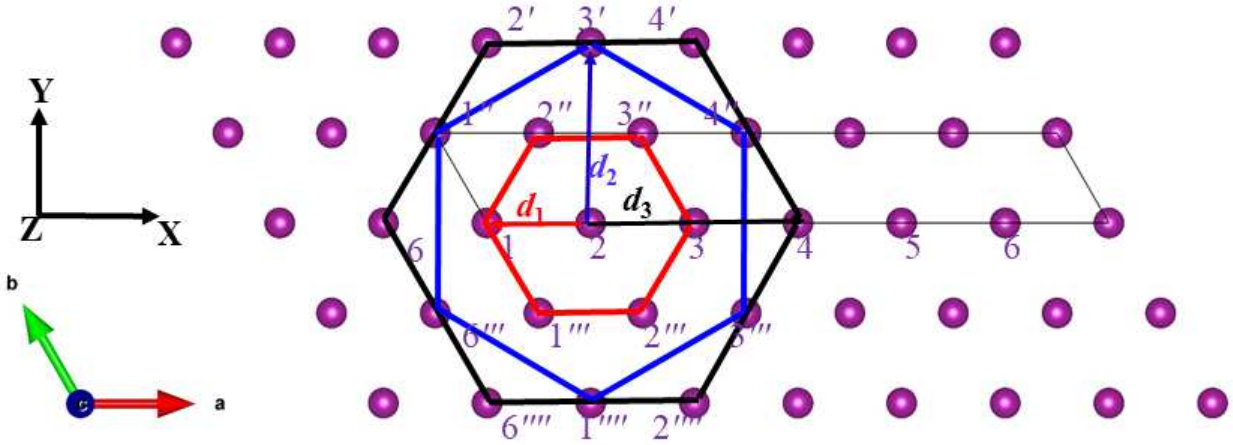

Figure S7. Top view of 6×1×1 supercell used to visualize intralayer contributions into DMI for the Mn layer. For clarity only the Mn atoms are shown here

D. The nearest-, next-nearest-, and third-nearest-neighbor DMI d_i (i = 1, 2 and 3)

Using Eqs. (S13), (S20), and (S27), which corresponds to the total DMI energy of 4×1×1, 5×1×1 and 6×1×1 supercell, respectively, we can get the d_i (i = 1, 2 and 3) as follows:

$$d_1 = 0.2412\Delta E_{\mathrm{DMI},\,1} - 0.1641\Delta E_{\mathrm{DMI},\,2} + 0.0287\Delta E_{\mathrm{DMI},\,3} \quad (28)$$

$$d_2 = -0.2734\Delta E_{\mathrm{DMI},\,1} + 0.2843\Delta E_{\mathrm{DMI},\,2} - 0.0497\Delta E_{\mathrm{DMI},\,3} \quad (29)$$

$$d_3 = 0.0745\Delta E_{\mathrm{DMI},\,1} - 0.1641\Delta E_{\mathrm{DMI},\,2} + 0.0928\Delta E_{\mathrm{DMI},\,3} \quad (30)$$

Part V. The study of stabilization of spin textures for MnSeTe monolayer under increased biaxial strain and temperature.

In order to justify the stabilization of the strain-induced magnetic phases in our work, we explore the temperature influence on spin textures under tensile and compressive strain as shown in Figure S8 and S9, respectively. As the temperature increases, one can see that the images of ferromagnetic skyrmion, skyrmionium, bimeron, and antiferromagnetic spin spiral in MnSeTe all begin to be less well defined above about 50 K and become more and more blurred up to 150 K. The blurring expresses the destabilization of the chiral spin textures by thermal fluctuations.

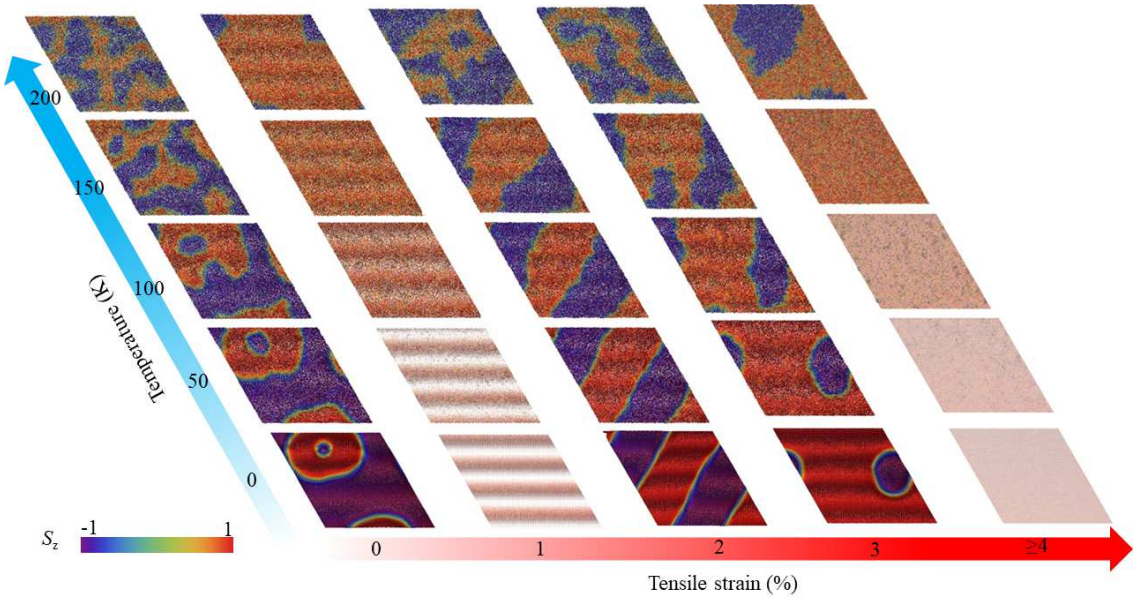

Figure S8. Distinct phase diagram of spin textures for MnSeTe monolayer under increased tensile strains and temperature.

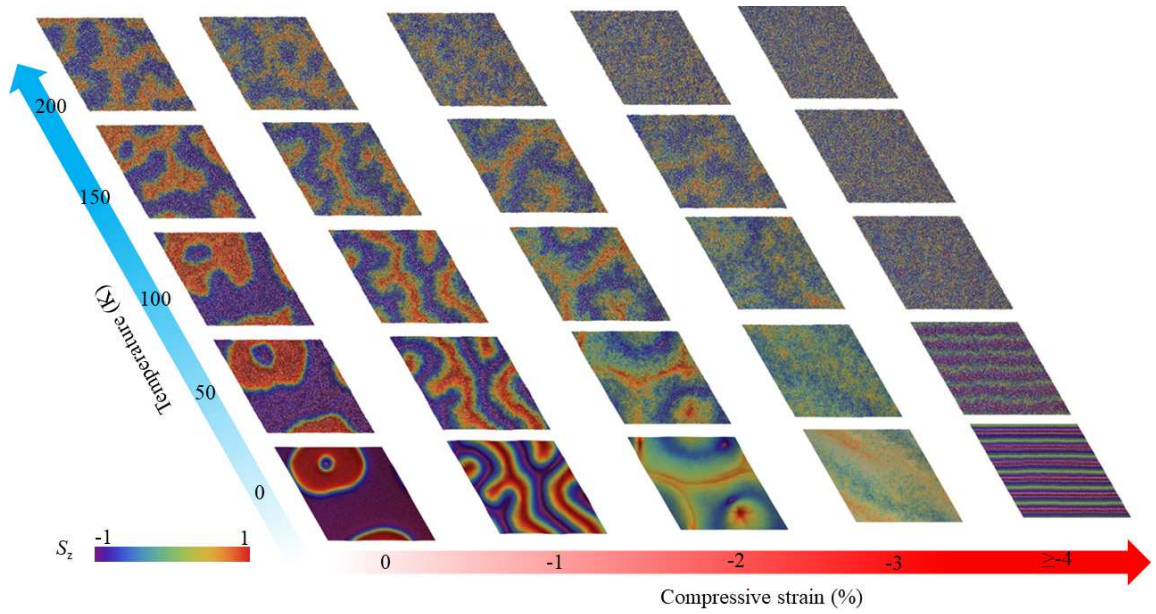

Figure S9. Distinct phase diagram of spin textures for MnSeTe monolayer under increased compressive strains and temperature.

Part V. The negligible effect of the dipole-dipole interaction on the magnetic structures of MnSeTe monolayer

The calculated effective magnetic anisotropy energy of the dipole-dipole interaction in the MnSeTe monolayer is only 0.11 meV/unit cell, which is much weaker as compared to the exchange coupling and the DMI. We have also performed the simulations without and with dipole-dipole interaction as shown in the Figure S10 for the pristine MnSeTe monolayer. We can find that similar skyrmion state emerges in both cases. It is thus that the dipole-dipole interaction can be neglected in the simulations.

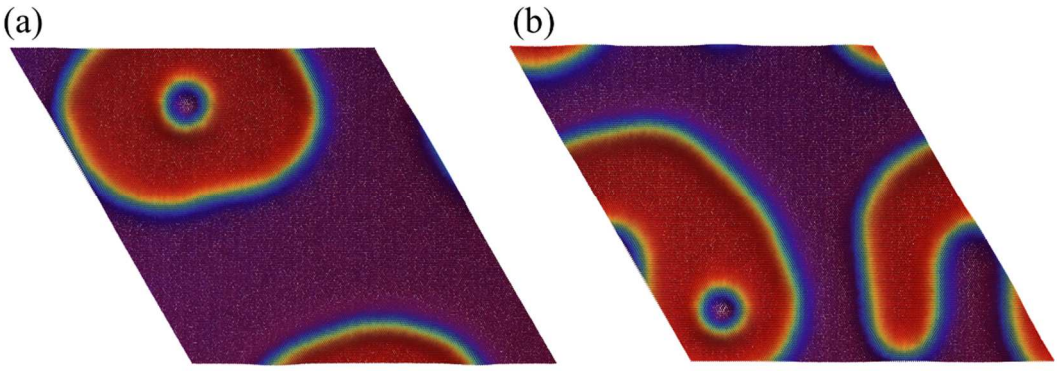

Figure S10. The simulated magnetic structures in the pristine MnSeTe monolayer (a) without and (b) with the dipole-dipole interaction.